Concluding Remarks

Several important points emerge from this theoretical study.

1. For PN and its neutral and singly charged isoelectronic analogues, the calculated equilibrium geometries (at MP3/6-311G(MC)(d)) and dissociation energies (at MP4/6-311G-(MC)(3d2f)) are uniformly in very good agreement with experimental values, with mean absolute errors being ±0.008 Å and 6 kJ mol^{-1}, respectively. Many of our calculated dissociation energies represent the most reliable values yet reported.

2. The dication analogues of PN, namely, SO^{2+}, NCl^{2+}, PF^{2+}, CAr^{2+}, and $SiNe^{2+}$, are all predicted to be experimentally observable species in the gas phase. The SO^{2+}, NCl^{2+}, and CAr^{2+} dications are calculated to be kinetically stable species with large barriers inhibiting the exothermic charge-separation reactions. The PF^{2+} and $SiNe^{2+}$ dications are found not only to be kinetically stable but also to be thermodynamically stable species. The doubly charged PF^{2+} ion is predicted to have a particularly large dissociation energy (D_0) of 458 kJ mol^{-1}.

3. Except for the neon-containing species, all the doubly and triply charged ions are characterized by short bonds in spite of strong Coulomb repulsion. In the case of SO^{2+}, the calculated equilibrium bond length (1.398 Å) may well be the shortest between any first-row atom and second-row atom.

4. Despite the availability of extremely exothermic fragmentation processes, the triply charged ions SF^{3+} and PNe^{3+} are predicted to have sizable well depths and thus should be experimentally accessible species in the gas phase. On the other hand, the OCl^{3+} and NAr^{3+} trications are predicted to lie in shallow potential wells.

5. The other highly charged species, FCl^{4+}, OAr^{4+}, SNe^{4+}, FAr^{5+}, $ClNe^{5+}$, and $ArNe^{6+}$, exhibit purely repulsive ground-state potential energy curves; i.e., they possess no bound equilibrium structures in their ground states.

6. The fragmentation of the multiply charged cations is well described by the recently introduced avoided crossing with diabatic coupling and polarization (ACDCP) model. The predicted transition structure bond lengths and kinetic energy releases are in satisfactory agreement with the directly calculated CASSCF/6-311G(MC)(d) values.

Acknowledgment. We gratefully acknowledge a generous allocation of time on the Fujitsu FACOM VP-100 of the Australian National University Supercomputer Facility. We are indebted to Dr. Brian Smith for advice and assistance in obtaining the spectroscopic constants.

Studies with $ClONO_2$: Thermal Dissociation Rate and Catalytic Conversion to NO Using an NO/O_3 Chemiluminescence Detector

L. C. Anderson[†] and D. W. Fahey*

National Oceanic and Atmospheric Administration, Aeronomy Laboratory, 325 Broadway R/E/AL6, Boulder, Colorado 80303 *(Received: December 27, 1988; In Final Form: August 7, 1989)*

A NO/O_3 chemiluminescence detector equipped with a gold catalyst is adapted to provide a measure of the thermal decomposition rate of $ClONO_2$ in an N_2/O_2 gas mixture and, in a related way, provide the absolute concentration of $ClONO_2$ in a flowing gas stream. The approach is to add $ClONO_2$, in the parts per million by volume (ppmv) range, to the flow stream of the detector in the presence of excess NO. As the sample is heated, $ClONO_2$ is thermally dissociated and the subsequent scavenging reaction of ClO with NO produces Cl and NO_2. Cl goes on to react with $ClONO_2$ to form NO_3 which, in turn, reacts with NO to produce NO_2. The loss of NO from the flow is precisely monitored downstream in the detector by the change in the chemiluminescence produced in the reaction of NO with reagent O_3. If the reaction rates with NO are given, the NO loss at a fixed temperature can be modeled to yield a dissociation rate constant for $ClONO_2$. Results were obtained for temperatures between 353 and 413 K and for pressures in the range of 66-160 Torr (8.8-21.3 kPa). The data is best fit by the expression $10^{-6.16}\exp(-90.7\text{ kJ mol}^{-1}/RT)$ cm^3 s^{-1} molecule^{-1}, which is in good agreement with earlier results. When combined with the rate constant for the association reaction of ClO and NO_2, these results yield a larger equilibrium constant for the reaction than indicated in previous direct measurements. A value for $\Delta H_f°_{289.15}$ for $ClONO_2$ of 22.9 kJ mol^{-1} is obtained from a third-law thermochemical analysis of the data. The initial $ClONO_2$ concentration in the sample is assumed to equal the absolute loss of NO measured when the dissociation and scavenging reactions have gone to completion. This affords the opportunity to calibrate the efficiency of other methods for the detection of $ClONO_2$. Results are presented for the conversion efficiency of $ClONO_2$ to NO found for a gold catalyst at 573 K with CO present as a reducing agent.

Introduction

The formation of $ClONO_2$ in reaction 1 with M = N_2 or O_2 has been well studied as a function of pressure and temperature with good agreement reached among several investigators.[1-6]

$$ClO + NO_2 + M \rightarrow ClONO_2 + M \quad (1)$$

$$ClONO_2 + M \rightarrow ClO + NO_2 + M \quad (-1)$$

In contrast, the decomposition rate, k_{-1}, has been measured by one group.[7,8] The accepted enthalpy of formation of $ClONO_2$ at 298 K of 26.4 kJ mol^{-1} is known from measured heats of reaction.[9,10] The equilibrium constant, k_1/k_{-1}, is higher than that derived from the enthalpy of $ClONO_2$. The difference can be resolved with a ~4 kJ mol^{-1} reduction in the enthalpy of formation of $ClONO_2$ or a factor of 3-4 increase in the value of k_{-1}. The discrepancy was initially attributed to the formation of $ClONO_2$ isomers.[6,11] Several later studies, however, found no evidence

[†] Also with Cooperative Institute for Research in Environmental Sciences, University of Colorado, Boulder, CO 80309.

(1) Lee, Y. P; Stimpfle, R. M.; Perry, R. A.; Mucha, J. A.; Evenson, K. M.; Jennings, D. A.; Howard, C. J. *Int. J. Chem. Kin.* **1982**, *14*, 711.
(2) Zahniser, M. S.; Chang, J.; Kaufman, F. *J. Chem. Phys.* **1977**, *67*, 997.
(3) Leu, M. T.; Lin, C. L.; DeMore, W. B. *J. Phys. Chem.* **1977**, *81*, 190.
(4) Birks, J. W.; Shoemaker, B.; Leck, T. J.; Borders, R. A.; Hart, L. J. *J. Chem. Phys.* **1977**, *66*, 4591.
(5) Cox, R. A.; Lewis, R. *J. Chem. Soc., Faraday Trans. 1* **1979**, *75*, 2649.
(6) Molina, M. J.; Molina, L. T.; Ishiwata, T. *J. Phys. Chem.* **1980**, *84*, 3100.
(7) Schonle, G.; Knauth, H. D.; Schindler, R. N. *J. Phys. Chem.* **1979**, *83*, 3297.
(8) Knauth, H. D. *Ber. Bunsen-Ges. Phys. Chem.* **1978**, *82*, 212.
(9) Alqasmi, R.; Knauth, H. D.; Rohlack, D. *Ber. Bunsen-Ges. Phys. Chem.* **1978**, *82*, 217.
(10) Knauth, H. D.; Martin, H.; Stockman, W. *Z. Naturforsch.* **1974**, *29a*, 200.

0022-3654/90/2094-0644$02.50/0

of additional channels in reaction 1.[12-14] If the agreement among the measurements of k_1 is meaningful and no isomers are formed, an error exists in either the measurement of the enthalpy or of k_{-1} or both. In this paper, we present new measurements of k_{-1} over the temperature range of 353–413 K at pressures of an N_2/O_2 mixture below 160 Torr (21 kPa). The values are in good agreement with earlier measurements summarized by Schonle et al.[7] A third-law analysis of the rate data confirms a lower enthalpy of formation for $ClONO_2$.

A unique feature of this study is the use of the detection of trace levels of NO. The NO detector relies on the high sensitivity and selectivity of the chemiluminescence reaction of NO with added O_3 in a flow of synthetic air. The reaction is carried out in an excess of O_3, thereby producing chemiluminescence proportional to NO in the sample. The specific instrument configuration used is similar to that developed for the measurement of ambient NO in the atmosphere with detection limits <0.01 parts per billion by volume (ppbv) for a 1-s integration [see, for example, McFarland et al.[15]]. When a sample flow containing $ClONO_2$ is heated, dissociation occurs producing ClO and NO_2. The ClO product is scavenged by NO as

$$ClO + NO \rightarrow Cl + NO_2 \quad (2)$$

The Cl product in turn reacts with $ClONO_2$

$$Cl + ClONO_2 \rightarrow Cl_2 + NO_3 \quad (3)$$

$$NO + NO_3 \rightarrow 2NO_2 \quad (4)$$

resulting in further loss of NO and $ClONO_2$. The loss of NO is measured accurately by the chemiluminescence detector since NO_2 and $ClONO_2$ have no intrinsic response. The dissociation rate of $ClONO_2$, k_{-1}, is determined by modeling the absolute concentration change in NO with increasing temperature for known reaction time and pressure.

If the dissociation and scavenging reactions are allowed to reach completion, the initial concentration or mixing ratio of $ClONO_2$ can be determined from the change in the NO concentration. This result provides an opportunity to calibrate the absolute efficiency of a detection method for $ClONO_2$. An important motivation for this study was to perform such a calibration for the catalytic conversion of $ClONO_2$ to NO on a gold surface with CO as a reducing agent. High conversion efficiency on gold has been noted for other reactive odd-nitrogen species, such as NO_2, N_2O_5, and HNO_3.[16] In the N_2O_5 study, a thermal dissociation and scavenging approach similar to that described here for $ClONO_2$ was used successfully.[17] The efficiency of $ClONO_2$ conversion is of interest due to recent measurements of the sum of reactive odd-nitrogen species, NO_y, made in the Antarctic stratosphere using a gold catalyst.[18] The results discussed below show near unity conversion efficiency for temperatures above 573 K.

Source/Detector Apparatus

The apparatus shown in Figures 1 and 2 consists of a $ClONO_2$ source and thermal dissociator tube attached to a chemiluminescence detector equipped with catalytic and photolytic converters. Since a constant sample flow of synthetic air (20% O_2, 80% N_2) is maintained throughout the various components, the system is similar in concept to a flow tube reactor. A measurement

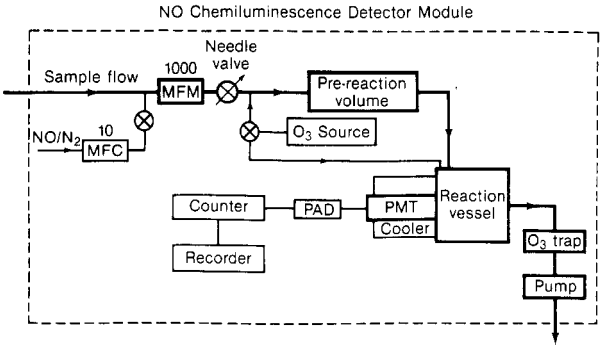

Figure 1. Schematic of the NO/O_3 chemiluminescence module. The bold line indicates the main sample flow of synthetic air through the module. The photons produced in the reaction are monitored with a photomultiplier tube (PMT) and counted with a pulse amplifier–discriminator (PAD) and counter. The reagent O_3 flow is diverted to the prereaction volume to measure the background photon signal. The flows of the calibration gas and sample are measured with a mass flow controller (MFC) and mass flow meter (MFM), respectively.

in the system is the steady-state detector signal obtained for well-defined or stable values of the various residence and reaction times throughout the system.

Chemiluminescence Detector System. The chemiluminescence detector system, shown in Figure 1, is designed to give an accurate and precise measure of the NO mixing ratio in a sample flow near 1000 sccm (STP (273 K, 1 atm) cm^3 min^{-1}). The detector utilizes the reaction of NO and reagent O_3 to produce NO_2 in the $^2B_1$ excited state. The relaxation of the excited state occurs through collisional quenching or through photon emission in a wavelength band centered near 1 μm. The photon count rate from a photomultiplier tube is linearly proportional to the mixing ratio of NO in the reaction volume of the detector at constant sample flow. The present detector is engineered to achieve a detection limit in atmospheric measurements of 0.01 ppbv for a 1-s integration.[15,19,20] Reagent O_3 is produced in a silent discharge ozonizer (4–5% by volume in 200 sccm) and added to the sample flow at the inlet to the detector reaction volume or at the entrance to a prereaction volume used to obtain the instrument zero. The detector response to NO is calibrated by standard addition of mixtures of NO in N_2 that are certified as Standard Reference Material [National Institute of Standards and Technology, Gaithersburg, MD].

The gold converter catalyst is located in the sample flow line upstream of the NO detector as shown in Figure 2. With added CO, NO_y component species, $(NO_y)_i$, are converted to NO in the proposed reaction

$$(NO_y)_i + CO = NO + CO_2 + \text{products} \quad (5)$$

The quantitative conversion of key species and the assessment of interferents in the conversion process are discussed by Fahey et al.[16] and Bollinger et al.[20] The converter is in the form of a thin-walled Au tube (0.48 cm id and 35 cm length) with a volume purity of 99.99%. The tube is uniformly heated in a copper block containing cartridge heaters with the temperature of the block monitored at midlength. High-purity CO reducing agent is added to the sample flow upstream of the converter to provide a mixing ratio of 0.3%.

A Pyrex photolysis cell is also located in the main sample flow line upstream of the NO detector. In the presence of near UV light from a Xe arc lamp, NO_2 is converted to NO as[15,19]

$$NO_2 + h\nu = NO + O \quad (6)$$

The 420-cm^3 cylindrical cell provides a path length of 53 cm. The conversion efficiency of trace levels of NO_2 derived from the NO standard is typically 40% at 100 Torr total pressure.

(11) Chang, J. S.; Baldwin, A. C.; Golden, D. M. *J. Chem. Phys.* **1979**, *71*, 2021.
(12) Margitan, J. J. *J. Geophys. Res.* **1983**, *88*, 5416.
(13) Cox, R. A.; Burrows, J. P.; Coker, G. B. *Int. J. Chem. Kin.* **1984**, *16*, 445.
(14) Burrows, J. P.; Griffith, D. W. T.; Moortgat, G. K.; Tyndall, G. S. *J. Phys. Chem.* **1985**, *89*, 266.
(15) McFarland, M.; Ridley, B. A.; Proffitt, M. H.; Albritton, D. L.; Thompson, T. L.; Harrop, W. J.; Winkler, R. H.; Schmeltekopf, A. L. *J. Geophys. Res.* **1986**, *91*, 5421.
(16) Fahey, D. W.; Eubank, C. S.; Hubler, G.; Fehsenfeld, F. C. *J. Atmos. Chem.* **1985**, *3*, 435.
(17) Fahey, D. W.; Eubank, C. S.; Hubler, G.; Fehsenfeld, F. C. *Atmos. Environ.* **1985**, *19*, 1883.
(18) Fahey, D. W.; Murphy, D. M.; Kelly, K. K.; Ko, M. K. W.; Profitt, M. H.; Eubank, C. S.; Ferry, G. V.; Loewenstein, M.; Chan, K. R. *J. Geophys. Res.* **1989**, *94*, 11299.
(19) Kley, D.; McFarland, M. *Atmos. Technol.* **1980**, *12*, 63.
(20) Bollinger, M. J. Chemiluminescent measurements of the oxides of Nitrogen in the clean troposphere and atmospheric chemistry implications. Ph.D. thesis, University of Colorado, Boulder, CO, 1982.

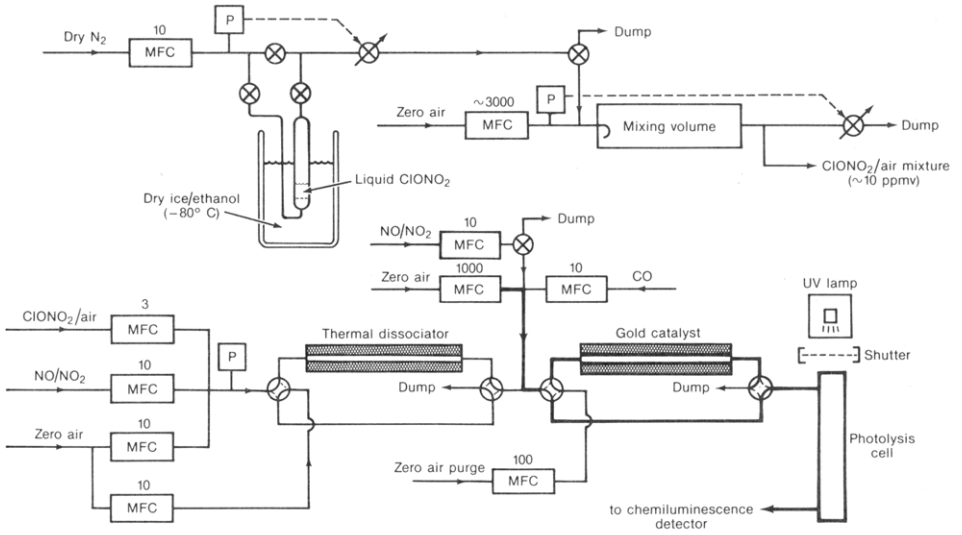

Figure 2. Schematic of the $ClONO_2$ source and the configuration of the thermal dissociator, gold catalytic converter, and UV photolysis tube. Mass flow controllers are designated by MFC with the nominal flow indicated as sccm (STP (1 atm, 0 °C) cm^3 min^{-1}) by the number above each unit. Pressure transducers are denoted by P and valves as circles. The bold line indicates the main sample line that continues as input to the chemiluminescence detector shown in Figure 1. The four-way valves at each end of the dissociator and converter are used in pairs to remove either device from the flow system.

$ClONO_2$ Source. The $ClONO_2$ source is shown schematically in Figure 2. $ClONO_2$ is made as the product of the reaction

$$Cl_2O + N_2O_5 \rightarrow 2ClONO_2 \quad (7)$$

in a procedure described by Davidson et al.[21] The resulting faint yellow liquid is stored in the dark near 193 K in a glass trap in a dry ice/ethanol bath. The sample used in this study was prepared by J. A. Davidson (National Center for Atmospheric Research, Boulder, CO) by this method. In analysis of earlier samples prepared in an identical way, the total impurity level was found to be low (≪5%).[21] Specifically, the levels of ClNO, $ClNO_2$, HNO_3, N_2O_5, and NO_2 were not detectable in infrared and visible absorption. However, Cl_2 and ClO_2 were observed in UV absorption at levels <2%. N_2O_5, as well as N_2O_4, is unlikely to be present in the trap output at levels above 1% since the respective vapor pressures are significantly lower than that of $ClONO_2$.[17]

A 10 sccm flow of high-purity (>99.99%) N_2 gas eluted $ClONO_2$ vapor from the liquid. The N_2 flow first passed over molecular sieve held at 193 K to reduce water vapor and other impurities. A fritted disk in the liquid sample promoted saturation of the N_2 carrier gas at trap pressures typically between 900 and 1000 Torr. From the absolute measurements of $ClONO_2$ discussed below, the vapor pressure of $ClONO_2$ at trap temperatures can be inferred. Values in the range of 1.6 and 2.1 Torr are calculated for temperatures between 190.3 and 193 K. This is in fair agreement with more direct measurements of Ballard et al.[22] and Schack[23] of 1.4 ± 0.02 Torr at 197.2 K and 1 Torr at 193.4 K, respectively.

After exiting the trap, the $ClONO_2/N_2$ flow is diluted to parts per million by volume (ppmv) levels by addition to a larger flow of synthetic air. A reduction is necessary because NO standards used for the ClO scavenging reaction are conveniently available at ppmv levels and because the high sensitivity of the NO detector would result in unsuitably high count rates for the undiluted levels. A small fraction of this diluted $ClONO_2/N_2$ flow passes through a mass flow control device and into the thermal dissociator discussed below.

The $ClONO_2$ vapor sample after leaving the trap is exposed primarily to Teflon tubing and valves and to some stainless steel tubing. Some passivation of these surfaces is required when they are first exposed to $ClONO_2$. This is presumably due to trace levels of water and hydrocarbons in the system and perhaps the greater reactivity of stainless steel. The exposure of $ClONO_2$ to surfaces in the trap and dilution system is thought to produce HNO_3, thereby producing the NO_y impurity observed in the conversion study discussed below. Such conversion has been noted in other experimental configurations.[24]

Thermal Dissociator. The thermal dissociator is configured as a side arm of the main detector sample line as shown in Figure 2. The dissociator is a glass tube (0.38 cm i.d. × 35 cm) held in good thermal contact with an aluminum block containing cartridge heaters. The tube temperature is uniform within ±1 K along its length with the absolute value monitored at the block center with an accuracy of ±1 K.

The aspect ratio or length/diameter of the heated section of the tube is chosen to be large in order to minimize end effects in heating the gas flow to a steady-state temperature. The length required for the mean temperature of the gas entering the tube to reach 90% of the wall temperature is estimated to be less than ~1 cm at ~30 sccm, corresponding to less than 3% of the tube length.[25] The length is not a function of the tube radius but depends linearly on the mass flow. This entrance effect is compensated by a similar distance at the tube exit required for the gas to return to room temperature. Thus, the reaction time at the dissociator temperature is assumed to be equal to the residence time for a 35 cm length with an uncertainty of less than a few percent. The aspect ratio and total flow value are such that the pressure drop across the tube of <3 Torr is negligible and the Reynolds number is <10, well within the laminar flow regime.

Upstream of the dissociator are the addition points for the flow of the NO/N_2 calibration mixture (4.11 ± 0.12 ppmv) and an auxiliary flow of synthetic air. The NO mixing ratio in the dissociator is maintained larger than the $ClONO_2$ mixing ratio by controlling the separate dilution step of $ClONO_2$ after the trap. The air flow in the dissociator reduces the residence time and provides a purge flow in the dissociator when $ClONO_2$ and NO are not added to the system. The total flow in the dissociator tube is ~27 sccm yielding a residence time at 354 K of 0.6 s. The resulting ratio of N_2 to O_2 in the dissociator of 7.3 is significantly higher than air. Previous studies of k_{-1} with both N_2 and O_2 as the third body, M, report small differences.[1]

Thermal Dissociation Data. A typical data run began with the addition of $ClONO_2$ to the thermal dissociator held at room temperature (~300 K). The response of the detector to this addition is negligible, indicating that reaction of O_3 with $ClONO_2$

(21) Davidson, J. A.; Cantrell, C. A.; Shetter, R. E.; McDaniel, A. H.; Calvert, J. G. *J. Geophys. Res.* **1987**, *92*, 10921.
(22) Ballard, J.; Johnston, W. B.; Gunson, M. R. *J. Geophys. Res.* **1988**, *93*, 1659.
(23) Schack, C. J. *Inorg. Chem.* **1967**, *6*, 1938.
(24) Burrows, J. P.; Tyndall, G. S.; Moortgat, G. K. *J. Phys. Chem.* **1988**, *92*, 4340.
(25) Gilbert, M. *Combust Flame* **1958**, *2*, 149.

TABLE I: Results for $\Delta\mu_{NO}$ (ppmv) as a Function of T (K)

Dissociator Conditions			
length = 35 cm		total flow = 26.8 sccm	
radius = 0.19 cm		μ_{N_2}/μ_{O_2} = 7.3	
length/radius = 184		μ_{NO} = 1.64 ppmv	

			$\Delta\mu_{NO}$			
P, Torr	P, kPa	μ_{ClONO_2}, ppmv	353 K	373 K	393 K	413 K
66	8.80	1.170	0.102	0.304	0.715	1.050
70	9.33	0.892	0.068	0.219	0.570	0.821
88	11.73	1.527	0.188	0.583	1.190	1.474
117	15.60	1.245	0.194	0.661	1.128	
160	21.33	1.426	0.360	1.041	1.386	

[a] The value of μ_{ClONO_2} for each run is the initial mixing ratio of $ClONO_2$ as determined from $\Delta\mu_{NO}$ measured at the completion temperature.

or other impurities from the trap does not produce chemiluminescence. As the next step, the NO/N_2 calibration flow is added to the dissociator. The presence of $ClONO_2$ does not alter the detector response to NO addition because the reaction of $ClONO_2$ with NO is slow and because the ClO concentration from the $[ClONO_2]/[ClO][NO_2]$ equilibrium is negligible at 298 K. If the results of Schonle et al.[7] and Margitan[12] are used for k_{-1} and k_1, respectively, the equilibrium dissociation fractions are less than 2% below 250 Torr at 298 K.

As the temperature of the dissociator is increased above 300 K, the $ClONO_2$ equilibrium shifts to favor the dissociation products ClO and NO_2. With NO present, ClO will react with NO in reaction 2 at a fast rate, reducing the NO mixing ratio and, therefore, the detector signal. At some temperature the dissociation and subsequent reactions reach completion, where further temperature increases produce no further loss of NO. This completion temperature is between 400 and 450 K for the range of dissociator conditions. The absolute change in the NO mixing ratio, defined as $\Delta\mu_{NO}$, when measured at or above the completion temperature is assumed to be equal to the mixing ratio of $ClONO_2$, μ_{ClONO_2}, present at the inlet of the dissociator. This is strongly supported in the model of dissociation and scavenging kinetics discussed below. A typical run is made at constant pressure and consists of up to four measurements of the NO loss at selected dissociator temperatures. The μ_{ClONO_2} and $\Delta\mu_{NO}$ data are shown in Table I for all the runs.

The simple kinetics for dissociating $ClONO_2$ are supported by several observations. First, the results of the model presented below suggest that, above the completion temperature, the NO loss in the dissociator leads to production of NO_2, ClONO, and $ClNO_2$. As a representative example, at 70 Torr and 413 K, the fractions produced are 0.9, 0.03, and 0.15, respectively. Using the photolysis technique described above, ~>90% of the expected NO_2 is routinely observed. Second, at and above the completion temperature, no variation of $\Delta\mu_{NO}$ is observed in several runs when the dissociator pressure is increased by as much as a factor of 3. Finally, in a similar check, no change in the value of $\Delta\mu_{NO}$ is observed when the initial NO mixing ratio is increased by as much as 60%.

Dissociation Rate

The determination of k_{-1} at some temperature, T, and pressure, P, from a measure of $\Delta\mu_{NO}$ in the thermal dissociator requires the application of a simple kinetic model. The model reaction set is listed in Table II along with the rate constant expressions adopted. The solution to a set of coupled differential equations describes the change in concentration of each species along the combined length of the thermal dissociator and a short (~4 cm) section of tubing between the dissociator and the main sample line. The set is solved by replacing differential terms with finite differences and by using time steps chosen to limit the change in concentration of any species to a maximum of 1%. A rate constant is determined by adjusting the value of k_{-1} until the calculated change in NO over the combined tube length equals the observed change, $\Delta\mu_{NO}$, as listed in Table II. The adjustment iteration continues until the difference between the calculated and observed change is within 1.5% of the initial NO value. The resulting values of k_{-1} are shown in Table III.

The short section of tubing after the dissociator and before the sample line is included in the calculation because the concentrations of NO and ClO at the end of the dissociator are sufficient that NO continues to react to form NO_2. A length after the dissociator is not easily avoided because of fittings and a valve required in the connection to the main sample line. In the calculation, the temperature is assumed to change discontinuously to 300 K at the end of the dissociator. If the length of the tubing is reduced to zero in the calculation, k_{-1} values increased by an average of 7%.

After the dissociator, reactions in the main sample line are negligible in further reducing NO in all cases. This follows principally from the ~0.03 dilution of the reactants that occurs on addition to the 1000 sccm sample flow. As an option, the model can include reactions occurring on the surface of the gold catalyst as discussed below.

The sensitivity of the calculated k_{-1} values to the inclusion of specific reactions is easily checked with the model. As expected, the reaction pair

$$Cl + ClONO_2 \rightarrow Cl_2 + NO_3 \quad (3)$$

$$NO + NO_3 \rightarrow 2NO_2 \quad (4)$$

is the most important. Since k_3 is comparable to k_2, reaction 3

TABLE II: Reactions and Rate Constant Expressions Used in the Model To Calculate k_{-1}, Where T is the Temperature (K) and M the Third-Body Reactant[a]

		k,[b] cm^3 s^{-1} molecule^{-1}
1. $ClO + NO_2 + M \rightarrow ClONO_2 + M$	$k_0 = (1.8 \pm 0.3)(-31)(T/300)^{-(3.4\pm1)}$[d] $k_\infty = (1.5 \pm 0.7)(-11)(T/300)^{-(1.9\pm1.9)}$	4.77(-13)
-1. $ClONO_2 + M \rightarrow ClO + NO_2 + M$	$8.32(-6)\exp(-11820/T)$[c]	4.94(-23)
2. $ClO + NO \rightarrow Cl + NO_2$	$6.4(-12)\exp((290 \pm 100)/T)$	1.69(-11)
3. $Cl + ClONO_2 \rightarrow Cl_2 + NO_3$	$6.8(-12)\exp((160 \pm 200)/T)$	1.16(-11)
4. $NO + NO_3 \rightarrow NO_2 + NO_2$	$1.7(-11)\exp((150 \pm 100)/T)$	2.81(-11)
5. $Cl + ClNO \rightarrow Cl_2 + NO$	$6(-11)\exp((0+500,-250)/T)$	6(-11)
6. $Cl + NO \rightarrow ClNO$	$k_0 = (9.0 \pm 2)(-32)(T/300)^{-(1.6\pm0.5)}$	2.95(-13)
7. $Cl + NO_2 \rightarrow ClONO$	$k_0 = (1.3 \pm 0.2)(-30)(T/300)^{-(2.0\pm1)}$ $k_\infty = (1.0 \pm 0.5)(-10)(T/300)^{-(1.0\pm1)}$	3.43(-12)
$Cl + NO_2 \rightarrow ClNO_2$	$k_0 = (1.8 \pm 0.3)(-31)(T/300)^{-(2.0\pm1)}$ $k_\infty = (1.0 \pm 0.5)(-10)(T/300)^{-(1.0\pm1)}$	8.9(-13)

[a] Read $a(-b)$ or $(a)(-b)$ as $a \times 10^{-b}$. Rate constant and uncertainty expressions for reactions other than k_{-1} are from NASA.[28] [b] T = 298 K, P = 100 Torr. [c] Previous direct measurements of Schonle et al.[7] and Knauth[8] as reported in ref 7. Rate is low-pressure limit valid to within 5% below 210 Torr. [d] Three-body rate constants are fit to the expression[28]

$$k = \frac{k_0 M}{(1 + (k_0 M)/k_\infty)^{0.6}}(1 + [\log\{k_0 M/k_\infty\}]^2)^{-1}$$

where k_0 (cm^6 s^{-1}) and k_∞ (cm^3 s^{-1}) are the low- and high-pressure limits, respectively.

TABLE III: Calculated k_{-1} (cm^3 s^{-1} $molecule^{-1}$) Values as a Function of P and T in the Thermal Dissociator Corresponding to the Runs in Table I[a]

P, Torr	P, kPa	353 K	373 K	393 K	413 K
66	8.80	3.57(−20)[b]	1.50(−19)	6.14(−19)	1.80(−18)[b]
70	9.33	2.77(−20)	1.44(−19)	5.90(−19)	1.75(−18)[b]
88	11.73	3.09(−20)[b]	1.44(−19)	5.90(−19)	2.27(−18)
117	15.60	2.39(−20)	1.44(−19)	5.78(−19)	
160	21.33	2.39(−20)	1.44(−19)	6.27(−19)	

[a] The uncertainty in k_{-1} is estimated to be ±20%. Read $a(-b)$ as $a \times 10^{-b}$. [b] Data points discarded in the third-law analysis.

TABLE IV: Fractional Changes in the k_{-1} Values in Table III That Result When the Model Calculation is Redone with (a) k_3 and (b) k_5, k_6, and k_7 Set Equal to Zero

P, Torr	P, kPa	353 K	373 K	393 K	413 K
			a		
66	8.80	+0.99	+0.95	+0.76	+0.63
70	9.33	+0.97	+0.73	+0.75	+0.58
88	11.73	+0.93	+0.91	+0.68	+0.16
117	15.60	+0.84	+0.71	+0.47	
160	21.33	+0.99	+0.51	+0.06	
			b		
66	8.80	0.0	0.0	−0.06	−0.14
70	9.33	0.0	−0.01	−0.07	−0.10
88	11.73	0.0	0.0	−0.12	−0.22
117	15.60	0.0	−0.08	−0.22	
160	21.33	0.0	−0.19	−0.32	

substantially increases the loss rate of $ClONO_2$ under most conditions. As indicated by the values in Table IV, the changes in k_{-1} when k_3 is set equal to zero vary from no change to a factor of 2. The change systematically reduces to zero as T and P in the dissociator are increased at constant mass flow. This roughly follows the change in the ratio of the lifetime of $ClONO_2$ against dissociation to the residence time in the tube. At the lowest T and P values, the $ClONO_2$ lifetime is long compared to the residence time so that reaction 3 competes effectively with reaction 2. A fractional change of +0.97 in k_{-1} occurs in this case when k_3 is set to zero. As T and P values are increased, the decrease in the $ClONO_2$ lifetime reduces the effect of k_3 on the calculated value of k_{-1}.

Similarly, Table IV shows the effect of setting k_5, k_6, and k_7 to zero. In contrast to the discussion above, when the $ClONO_2$ lifetime is relatively long, the effect is small because the Cl concentration remains low. When the $ClONO_2$ lifetime is short, however, reactions 5–7 compete with reaction 3 for Cl, increasing the apparent dissociation rate for a given $\Delta\mu_{NO}$ value. In separate model runs using rate constants estimated from the association reaction rate and the equilibrium constant,[26] the dissociations of both $ClNO_2$ and ClONO were shown to have no effect on k_{-1}. Thus, any isomerization of ClONO to $ClNO_2$ will also have no effect on k_{-1}.

The change in k_{-1} from setting the formation rate of $ClONO_2$, k_1, to zero is generally small. Below 413 K, the fractional change is <+0.03, since the lifetime of $ClONO_2$ is longer than or comparable to the dissociator residence time. At 413 K, the fraction increases to as much as a +0.10 change.

The reaction

$$NO + ClONO_2 \rightarrow \text{products}$$

is not included in the model set. Measurements by Knauth[27] yield a reaction rate of 8.2 (−20) cm^3 s^{-1} $molecule^{-1}$ at 350 K which is approximately 5 times faster than the dissociation rate k_{-1}. However, the loss of $ClONO_2$ in this reaction is negligible under all conditions since the mixing ratio of NO in the dissociator is ~1 ppmv.

The propagation of errors in the calculated k_{-1} values must address both systematic and random sources. The largest contribution is a ±1 K temperature uncertainty that yields a 8 (±4)% change in k_{-1}. The second largest contribution is the uncertainty in the accepted rate values shown in Table I from the NASA evaluation.[28] When these rate constants are adjusted within the uncertainty range to maximize the calculated value of k_{-1}, the resulting change is 5 (±5)%, with the largest changes occurring at the highest temperatures. Uncertainties in the pressure of 1 Torr (0.13 kPa) and in the counting statistics of the detector yield changes of 2.5 (±3)% and 2 (±3)%, respectively. The uncertainty in the dissociator mass flows combine to give an uncertainty of ~2.5%. When added in quadrature, the contributions combine to give a net uncertainty in k_{-1} of ~±10%. To be conservative, we choose to quote a net uncertainty of ±20%.

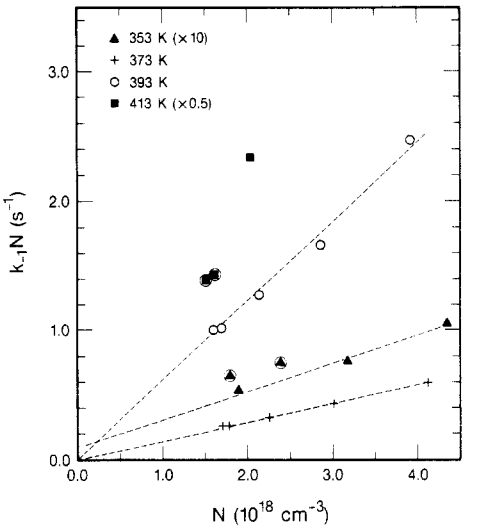

Figure 3. Plot of the pseudo-first-order rate constant, $k_{-1}N$, as a function of N, the gas number density in the thermal dissociator. The data points are grouped by temperature from the values in Table III. The circled points are those indicated as outliers in the third-law analysis as shown in Table VI. The lines are a hand-fit to the remaining points in each set.

The presence of an NO_y impurity in the sample is evident in the conversion efficiency tests presented below. Unfortunately, the impurity level is not known for the rate constant runs. The maximum impurity levels are expected to be similar to those measured for $ClONO_2$ samples prepared previous to this study as discussed above. The effect of the impurity in the model calculations cannot be determined without proper identification. However, if the variability of the impurity in the conversion tests is representative, the consistency observed in the rate constant determinations alone suggests that the impurity has negligible effect on the results. The most likely impurity, HNO_3, would produce a negligible effect at these temperatures due to its low reactivity with NO, NO_2, and other components.

As a internal consistency check of the k_{-1} values in Table III, Figure 3 shows the pseudo-first-order rate constant of the dissociation, $k_{-1}N$, as a function of N, where N is the number density in the tube. The points are grouped by temperature and are scaled appropriately to be included on a single graph. If the measurements have no relative systematic errors and no heterogeneous processes are involved in the dissociation, then each group of points should form a straight line with zero as an intercept. Care must be used in any interpretation here because the data are acquired at constant pressure. The data for 373 and 393 K fit such a line, whereas the remaining data sets have a nonzero intercept if all the points are included. The circled points in these latter sets indicate outliers in the third-law thermochemical analysis discussed below. If these points are excluded from the fits, the three remaining points in the 353 K set give an acceptable fit with near-zero intercept and the 413 K set is reduced to one point. Thus, the data appear self-consistent with simple kinetics and

(26) Patrick, R.; Golden, D. M. *Int. J. Chem. Kinet.* **1983**, *15*, 1189.
(27) Knauth, H.-D. *Ber. Bunsen-Ges. Phys. Chem.* **1978**, *82*, 428.
(28) NASA Panel for Data Evaluation, No. 8. "Chemical Kinetics and Photochemical Data for Use in Stratospheric Modeling"; Jet Propulsion Laboratory Publication 87-41, 1987.

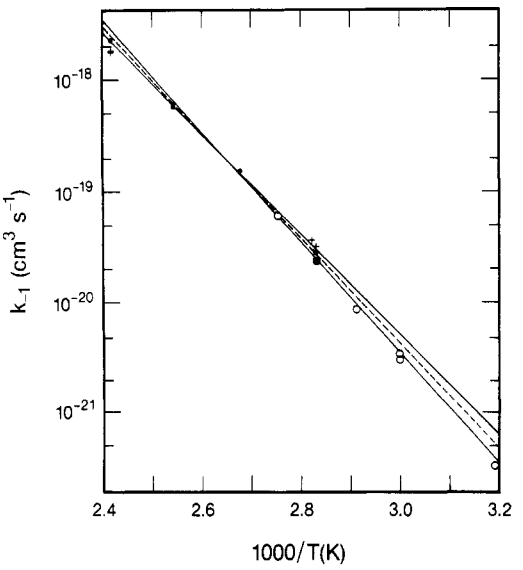

Figure 4. Plot of k_{-1} as a function of $1/T$ (K) for the data in Table III. The solid line with the lowest y intercept is a least-squares fit to all the data in this study while the dashed line is a similar fit that results when the points identified as outliers (crosses) in the third-law analysis are excluded. The remaining solid line is the fit to the present data less the outlying points and the data of Schonle et al.[7] and Knauth[8] (open symbols). The line parameters are given in Table V.

TABLE V: Comparison of k_{-1} Values for Various Groupings of Data[a]

	A, cm^3 s^{-1} molecule^{-1}	E_A, kJ mol^{-1}	T, K
1. present results[b]	$10^{-6.75\pm0.19}$	86.5 ± 1.4	353–413
2. present results[c]	$10^{-6.16\pm0.15}$	90.7 ± 1.1	353–413
3. Schonle et al.[7]	$10^{-5.08\pm0.1}$	98.3 ± 0.9	313–363
4. 2 and 3 combined	$10^{-5.56\pm0.12}$	95.1 ± 0.9	313–413

[a] The constants with indicated standard deviation result from a least-squares fit to the Arrhenius expression $A\exp(-E_A/RT)$, where E_A is the activation energy of the reaction and R is the gas constant, 8.314 J mol^{-1} K^{-1}. [b] All data. [c] Points discarded as a result of third-law analysis.

further suggest that heterogeneous processes are not important under these conditions.

The existence of outlying points in Table III can be seen directly from the data grouped by thermal dissociator temperature. In the low-pressure limit, k_{-1} should depend only on temperature as indicated in Table II. Schonle et al.[7] and Knauth[8] measure a slight falloff in k_{-1} from a second-order dependence below 200 Torr, consistent with measurements of Cox and Lewis[29] and Handwerk and Zellner[30] of the formation reaction rate, k_1, below 1 atm and near 350 K. Therefore, the apparent variation with pressure, especially at 353 and 413 K, is inconsistent with this limit. The outlying points are identified objectively in the third-law analysis presented below, reducing the discrepancy. Outlying points may be expected at the lowest and highest run temperatures because the signal precision is lowest at low temperatures and because the high temperatures are near the completion temperature in the dissociator.

The dependence of k_{-1} as a function of $1/T$ is shown in Figure 4 with the fit parameters listed in Table V. The data provide a good fit to an Arrhenius expression with a positive activation energy as expected from previous studies.[1] A comparison to the Schonle et al.[7] rate data is good considering the absolute uncertainties. The fit using both the Schonle et al. data and the present reduced data set is also included in the Table V.

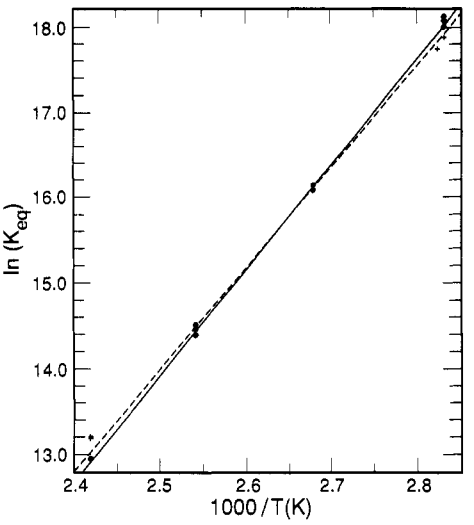

Figure 5. Plot of ln (K_{eq}) as derived from $k_1/(RTk_{-1})$ as a function of $1/T$ (K). The dashed line is a least-squares fit to all the data and the solid line is a similar fit that results when the points identified as outliers (crosses) in the third-law analysis are excluded. The parameters of the line fits are given in the text.

$ClONO_2$ Formation Enthalpy

The standard heat of formation of $ClONO_2$ at 298.15 K, $\Delta H_f^\circ{}_{298.15}$ ($ClONO_2$), can be calculated from the measured values of k_{-1} in both a second-law and third-law analysis. We chose to do both here based on the strong recommendation in Chase et al.[31] In the second-law analysis, the equilibrium constant of the reaction, K_{eq}, in standard-state units relates to the Gibbs free energy of reaction, $\Delta G_r^\circ = \Delta H_r^\circ - T\Delta S_r^\circ$, at temperature T as

$$K_{eq} = \frac{k_1}{k_{-1}}(RT)^{-1} = \exp(-\Delta G_r^\circ/RT) \quad (8)$$

Values of k_1 are derived from the expression given in Table II. The enthalpy of reaction, ΔH_r°, and the entropy of reaction, ΔS_r°, can be derived from the van't Hoff plot showing ln K_{eq} vs $1/T$. Figure 5 shows this plot using the present data where the dashed line is the least-squares fit to all of the data, yielding

$$\Delta H_r^\circ = -99.6 \text{ kJ mol}^{-1}$$
$$\Delta S_r^\circ = -132.7 \text{ J mol}^{-1} \text{ K}^{-1} \quad (9)$$

If the temperature dependences of ΔH_r° and ΔS_r° are known or assumed to be small, a value for $\Delta H_f^\circ{}_{298.15}(ClONO_2)$ can be derived from eq 9. Because of the uncertainty in the fit, however, we chose not to use this calculation in favor of the third-law analysis.

In the third-law analysis, each measurement of k_{-1} is used separately to derive a value of $\Delta H_r^\circ{}_{298.15}$ and $\Delta H_f^\circ{}_{298.15}(ClONO_2)$. As discussed by Chase et al.,[31] the relationship makes use of the Gibb's energy function as

$$\Delta H_r^\circ{}_{298.15} = -RT \ln [K_{eq}(T)] - \sum[-TS^\circ(T) + [H^\circ(T) - H^\circ(298)]] \quad (10)$$

where the sum is over products minus reactants of reaction 1. The quantities of S° and H° can be calculated from the spectroscopic constants or interpolated from the thermochemical compilation of Chase et al.[31] Since the compilation does not include $ClONO_2$, calculations of S° and H° were made using the spectroscopic constants of Miller et al.[32] A useful number from these calculations is the value

$$S^\circ{}_{298.15}(ClONO_2) = 302.382 \text{ J mol}^{-1} \text{ K}^{-1} \quad (11)$$

The input data for each run and the resulting values of $\Delta H_{r,298.15}$ and $\Delta H_f^\circ{}_{298.15}(ClONO_2)$ are shown in Table VI. The mean value

(29) Cox, R. A.; Lewis, R. *J. Chem. Soc., Faraday Trans. 1* **1979**, *75*, 2649.
(30) Handwerk, V.; Zellner, R. *Ber. Bunsen-Ges. Phys. Chem.* **1984**, *88*, 405.
(31) Chase, Jr., M. W.; Davies, C. A.; Downey, Jr., J. R.; Frurip, D. J.; McDonald, R. A.; Syverud, A. N. *J. Phys. Chem. Ref. Data* **1985**, *14*, 1.
(32) Miller, R. H.; Bernitt, D. L.; Hisatune, I. C. *Spectrochim. Acta* **1967**, *23A*, 223.

TABLE VI: Table of Input Data and Results for the Third-Law Analysis of the k_{-1} Values[a]

P, Torr	P, kPa	T, K	$1000/T$	k_{-1}, cm^3 s^{-1}	k_1, cm^6 s^{-1}	K_{eq}
70.0	9.33	353	2.83	2.77(−20)	8.96(−32)	6.73(7)
88.0	11.73	353	2.83	3.09(−20)	8.82(−32)	5.94(7)
117.0	15.60	353	2.83	2.39(−20)	8.62(−32)	7.50(7)
160.0	21.33	353	2.83	2.39(−20)	8.35(−32)	7.27(7)
66.5	8.87	354	2.82	3.57(−20)	8.91(−32)	5.18(7)
66.6	8.88	373	2.68	1.50(−19)	7.52(−32)	9.90(6)
70.0	9.33	373	2.68	1.44(−19)	7.50(−32)	1.03(7)
88.0	11.73	373	2.68	1.44(−19)	7.39(−32)	1.01(7)
117.0	15.60	373	2.68	1.44(−19)	7.23(−32)	9.88(6)
160.0	21.33	373	2.68	1.44(−19)	7.03(−32)	9.60(6)
66.0	8.80	393	2.54	6.14(−19)	6.34(−32)	1.93(6)
70.0	9.33	393	2.54	5.90(−19)	6.32(−32)	2.00(6)
88.0	11.73	393	2.54	5.90(−19)	6.24(−32)	1.98(6)
117.0	15.60	393	2.54	5.78(−19)	6.12(−32)	1.98(6)
160.0	21.33	393	2.54	6.27(−19)	5.96(−32)	1.78(6)
66.0	8.80	413	2.42	1.80(−18)	5.39(−32)	5.33(5)
70.0	9.33	413	2.42	1.75(−18)	5.38(−32)	5.46(5)
88.0	11.73	413	2.42	2.27(−18)	5.31(−32)	4.16(5)

$S°_{ClONO_2}$	$(H° - H°_{298.15})_{ClONO_2}$	$\Delta\Delta H_r°$	$\Delta H_r°_{298.15}$	$\Delta H_f°_{298.15}(ClONO_2)$	mean diff
314.444	3.923	0.096	−110.89	23.42	−0.65
314.444	3.923	0.096	−110.52	23.79	−1.02[b]
314.444	3.923	0.096	−111.21	23.11	−0.33
314.444	3.923	0.096	−111.12	23.20	−0.43
314.658	3.997	0.098	−110.43	23.89	−1.12[b]
318.578	5.423	0.164	−111.18	23.14	−0.36
318.578	5.423	0.164	−111.30	23.02	−0.25
318.578	5.423	0.164	−111.25	23.07	−0.29
318.578	5.423	0.164	−111.18	23.13	−0.36
318.578	5.423	0.164	−111.09	23.22	−0.45
322.582	6.957	0.248	−111.83	22.49	0.28
322.582	6.957	0.248	−111.94	22.37	0.40
322.582	6.957	0.248	−111.90	22.41	0.36
322.582	6.957	0.248	−111.90	22.41	0.36
322.582	6.957	0.248	−111.55	22.76	0.01
326.469	8.523	0.346	−113.07	21.24	1.53[b]
326.469	8.523	0.346	−113.16	21.53	1.62[b]
326.469	8.523	0.346	−112.24	22.09	0.68
			mean[c] −111.54 (±0.75)	22.77 (±0.75)	
			mean[d] −111.47 (±0.41)	22.85 (±0.41)	

[a] Read $a(-b)$ as $a \times 10^{-b}$. Entropy and enthalpy units are (J mol^{-1} K^{-1}) and (kJ mol^{-1}), respectively. k_1 calculated from the expression in Table I. K_{eq} in units of standard state at 100 kPa. $S°$ and $H°$ calculated from spectroscopic constants of Miller et al.[32] $\Delta\Delta H_r = \sum[H° - H°_{298.15}]$ for reaction 1 where the sum is over (products − reactants). $\Delta H_f°_{298.15}(ClONO_2) = \Delta H_r°_{298.15} + \Delta H_f°_{298.15}(ClO) + \Delta H_f°_{298.15}(NO_2) = \Delta H_r°_{298.15} + 134.31$ kJ mol^{-1}.[31] ±Values are ±1 standard deviation of the sample. Mean diff equals $[22.77 - \Delta H_f°_{298}(ClONO_2)]$(kJ mol^{-1}). [b] Points discarded. [c] All points. [d] With points discarded.

of $\Delta H_f°_{298.15}(ClONO_2)$ is 22.77 ± 0.75 kJ mol^{-1}, where the 1σ standard deviation indicates a general consistency within the data set. In the last column, which shows the difference between each individual value and the mean value, several points are clear outliers. If the four points (marked by *) differing by more than 1σ from the mean are excluded, the mean changes slightly to 22.85 kJ mol^{-1}, while the standard deviation is lowered by one-half to 0.41 kJ mol^{-1}. The four discarded points appear as outliers at the temperature extremes in Figures 4 and 5, as expected from the discussion above.

If the four outlying points are discarded in Figure 5, the new fit shown as the solid line yields the new values

$$\Delta H_r° = -103.6 \text{ kJ mol}^{-1}$$

$$\Delta S_r° = -143.5 \text{ J mol}^{-1} \text{ K}^{-1} \quad (12)$$

When eq 11 is combined with standard $S°$ values for NO_2 and ClO,[31] the entropy change in reaction 1 is calculated to be

$$\Delta S_r°_{298.15} = 302.382 - 240.034 - 226.648$$

$$= -164.300 \text{ (J mol}^{-1} \text{ K}^{-1}) \quad (13)$$

This value is in fair agreement with the value in eq 12.

The uncertainty in the mean value of $\Delta H_f°_{298.15}(ClONO_2)$ follows from several sources. The first is the standard deviation of ±0.41 kJ mol^{-1} in the reduced data set of 14 points. The second is the measurement of uncertainty in k_{-1}, estimated to be ±20%. A uniform increase in k_{-1} by 20% in Table VI alters the mean $\Delta H_f°_{298.15}(ClONO_2)$ value by ~+0.6 kJ mol^{-1}. A conservative estimate of the overall measurement error can be made as the sum of these two terms or ~±1 kJ mol^{-1}. The uncertainties in k_1 and $\Delta H_f°$ for NO_2 and ClO represent independent errors. By use of the expression in Table II and the range of dissociator conditions in Table I, the uncertainty in k_1 varies over the range (−30%, +60%). Since the agreement among the various studies is, in general, excellent for this reaction,[28] this range would seem to be an upper limit. A ±40% change in k_1 transforms to a change in $\Delta H_f°_{298.15}(ClONO_2)$ of (−1, +1.7) kJ mol^{-1}. The uncertainties in $\Delta H_f°_{298.15}$ are ±0.84 and ±0.21 kJ mol^{-1} for NO_2 and ClO, respectively.[31] If these latter values are added in quadrature to ±1 kJ mol^{-1} to derive a full uncertainty, the result is 22.9 (−1.7, +2.2) kJ mol^{-1}.

The current accepted value of 26.4 (±0.8) kJ mol^{-1} is somewhat larger than the present result, and outside the range of the combined uncertainties.[9] However, the quoted uncertainty does not include the independent uncertainties of $\Delta H_f°$ for NO_2, N_2O_4, and ClNO that are used in the calculation of $\Delta H_f(ClONO_2)$. If these sources are included, the actual uncertainty may be as large as ±2 kJ mol^{-1}. The added uncertainty reduces the importance of the apparent discrepancy between the thermochemical and kinetic measurements discussed in the Introduction.

Conversion of $ClONO_2$ to NO

At the completion temperature of ~450 K and above, the model results show that the dissociation and scavenging of $ClONO_2$ is complete and that $\Delta\mu_{NO}$ is equal to the initial μ_{ClONO2} in the

TABLE VII: Results for the Conversion Efficiency of $ClONO_2$ to NO, ξ_{ClONO_2}, Using a Heated Gold Catalyst with CO as a Reducing Agent As Determined by the Two Methods Described in the Text

		$D_3 - D_4$	$(D_5 - C)/(D_1 - D_2)$				
T, K	T, °C	7.3 kPa, 50 Torr	7.3 kPa, 50 Torr	9.3 kPa, 70 Torr	16.0 kPa, 120 Torr	26.7 kPa, 200 Torr	33.3 kPa, 250 Torr
473	200		(0.30)[a]				
548	275	1.00	0.94	0.97	0.95	0.94	
573	300	1.00	0.91	0.91	0.91		0.92
673	400	0.99	0.93	0.92	0.92		0.86
773	500	1.00	0.97		0.96		0.92

[a] Upper limit value.

dissociator within 2%. This result has the effect of "calibrating" the mass flow of $ClONO_2$ in the flow system and provides the basis for establishing the quantitative conversion efficiency of $ClONO_2$ to NO on the gold catalyst, defined as ξ_{ClONO2}.

Two methods of determining ξ_{ClONO2} result from combining the detector signals from five different modes of the system. In general, the chemiluminescence detector signal in any steady-state mode i, defined as D_i, is the product of the sensitivity to NO, S_{NO}, and the current mixing ratio of NO in the sample line, μ, as

$$D_i = S_{NO}\mu \tag{14}$$

As a simplification, S_{NO} is set to unity in the discussion below.

The first mode, D_1, is that obtained when a constant mixing ratio of NO, $\mu°$, used for the scavenging reaction is added to the system.

$$D_1 = \mu° \tag{15}$$

The second mode is obtained when the thermal dissociator temperature is then raised to the completion temperature of ~450 K and the catalyst is bypassed (see Figure 2). In this case the detector signal is lowered by $\Delta\mu_{NO}$ as

$$D_2 = D_1 - \Delta\mu_{NO} \tag{16}$$

The third mode is obtained when the catalyst is returned to the sample line. The signal increases by the conversion of the NO_2 dissociation product and the scavenging products NO_2, ClONO, and $ClNO_2$, all with assumed 100% efficiency, and by the conversion of any other NO_y species that are present as impurities, denoted as C.

$$D_3 = D_2 + 2\Delta\mu_{NO} + C \tag{17}$$

The fourth mode occurs when the NO and $ClONO_2$ flows are then diverted to bypass the thermal dissociator (see Figure 2), preventing any scavenging from occurring before the catalyst. The signal then has three components as

$$D_4 = D_1 + \xi_{ClONO_2}\mu_{ClONO_2} + C \tag{18}$$

where μ_{ClONO_2} is the mixing ratio of $ClONO_2$ in the sample line. The change between D_3 and D_4 can be accomplished with a minimum disturbance to the system. The change rapidly and quantitatively converts $ClONO_2$ to a mixture of NO_2, ClONO, and $ClNO_2$, all species assumed to have essentially unity conversion efficiency. By taking the difference and cancelling terms, we have

$$D_3 - D_4 = (1 - \xi_{ClONO_2})\Delta\mu_{NO} \tag{19}$$

Thus, any change in the signal must be attributed to a value of ξ_{ClONO_2} less than unity, scaled by the absolute value of $\Delta\mu_{NO}$. The results for 55 Torr (~7 kPa), the pressure of most interest for stratospheric measurements, are shown in Table VII. For all temperatures the signal change is less than 1%, corresponding to ξ_{ClONO_2} values >0.95.

Finally, the fifth mode of the system is the addition of only $ClONO_2$ to the catalyst. In this case, we have

$$D_5 = \xi_{ClONO_2}\mu_{ClONO_2} + C \tag{20}$$

Noting that $\mu_{ClONO_2} = \Delta\mu_{NO}$, it follows that

$$\xi_{ClONO_2} = (D_5 - C)/(D_1 - D_2) \tag{21}$$

which provides the second determination of ξ_{ClONO_2}. The values found over a range of temperatures and pressures are listed in Table VII. The values primarily range between 0.9 and 1.0. No particular trend is noted in either variable. The scatter is indicative of the stability of the source and detector over the time interval necessary for these measurements. The impurity values, C, used in the determinations varied from 3% to 30% of the value of $\Delta\mu_{NO}$. The only effect of $C \neq 0$ in this determination is to reduce the precision of the conversion efficiency calculations.

From the high values of ξ_{ClONO_2} and the basic agreement of the two methods, we conclude that $ClONO_2$ reliably converts to NO on a heated gold surface in the presence of CO. This result can be compared to the model results when the conversion step is added to the dissociation reactions. In general, conversion is assumed to occur at the walls of the gold tube with unity efficiency, but transport to the walls is diffusion limited.[33] In the model, the wall reactivity is input as a variable. With high wall reactivity, conversion of $ClONO_2$ directly to NO is >95% for temperatures above 348 K. With the wall reactivity set to zero for $ClONO_2$, $ClONO_2$ must first dissociate to form NO_2 which subsequently reacts at the wall. In this case, 95% conversion is predicted by the model only for temperatures above ~498 K. From the measurements listed in Table VII, the conversion is observed to drop off substantially between 523 and 473 K. This suggests that $ClONO_2$ does not convert directly to NO but must first dissociate to form NO_2.

Conclusions

The NO/O_3 chemiluminescence detector coupled with a scavenging reaction scheme is shown to provide a new measurement of the dissociation rate of $ClONO_2$ and to provide the basis for demonstrating the quantitative conversion of $ClONO_2$ to NO. The data set of dissociation rates, reduced by removing the outlying points, is in good agreement with previous measurements of Schonle et al.[7] over a similar temperature and pressure range. Such agreement is especially satisfying given the widely differing techniques.

Given the quite good agreement among several groups for the rate of the association reaction, it seems most appropriate to combine the kinetic measurements to calculate K_{eq} and $\Delta H_f°_{298.15}(ClONO_2)$. The result of 22.9 (−1.7, +2.2) kJ mol^{-1}, including all uncertainties, is substantially less than the current value of 26.4 ± 0.8 kJ mol^{-1}.

Changes in the kinetics and thermochemistry of $ClONO_2$ are of current interest due to its role as a reservoir of reactive Cl in the stratosphere. The largest changes in the $ClONO_2$ reservoir occur with production from the ClO + NO_2 association reaction and destruction from UV photodissociation. The lifetime against thermal dissociation at 50 mbar and 220 K is hundreds of years. Therefore, small changes of the dissociation rate constant and changes in $\Delta H_f°$ of a few kilojoules per mole have little consequence in stratospheric photochemistry.

The measurements here confirm the expectation that $ClONO_2$ can be effectively converted to NO with a heated gold catalyst. This may be of interest to laboratory kineticists who want to exploit this as a detection method. In the current effort to understand polar ozone loss at high latitudes, the knowledge that $ClONO_2$

(33) Bollinger, M. J.; Sievers, R. E.; Fahey, D. W.; Fehsenfeld, F. C. *Anal. Chem.* **1983**, *55*, 1980.

is adequately detected in measurements of NO_y will contribute significantly to the proper modeling of the phenomenon.

Acknowledgment. We are especially indebted to J. A. Davidson and C. A. Cantrell of the National Center for Atmospheric Research for providing the sample of $ClONO_2$ used throughout this study. The counsel of A. R. Ravishankara, C. J. Howard, and G. S. Tyndall of the Aeronomy Laboratory concerning the experimental approach and the use of thermochemical data was of great value.

Kinetics of Bimolecular Recombination Processes with Trapping

Jayendran C. Rasaiah,

Department of Chemistry, University of Maine, Orono, Maine 04469

Joseph B. Hubbard,*

Center for Chemical Engineering, Thermophysics Division, National Institute of Standards and Technology, Gaithersburg, Maryland 20899

Robert J. Rubin,

Laboratory for Molecular Biology, National Institutes of Health (NIDDK), Bethesda, Maryland 20892

and Song Hi Lee

Department of Chemistry, Kyung Sung University, Pusan, Korea 608-023 *(Received: March 17, 1989; In Final Form: June 30, 1989)*

We report the results of a computer simulation and analysis of diffusion-controlled bimolecular recombination on a two-dimensional square lattice with the possibility of trapping. The following reactions are considered: (Ia) $A + A \rightarrow$ annihilation, (Ib) $A + T \rightarrow A_T$, (Ic) $A_T + A \rightarrow T$; (IIa) $A + A \rightarrow$ annihilation, (IIb) $A \rightarrow A_T$, (IIc) $A_T + A \rightarrow$ annihilation. Reaction I refers to recombination with bimolecular trapping (b), while reaction II refers to recombination with unimolecular trapping (b). In either case the time dependence of the trapped population (A_T) is described remarkably well by a mean field theory, while the free population (A) decays as a stretched exponential at long times ($\exp(-t^{\alpha})$, $\alpha \sim {}^1/_2$). However, it is possible to distinguish between mechanisms I and II simply by monitoring a single particle density (A or A_T) for a range of initial conditions.

I. Introduction

Within the past few years there seems to have been a renaissance in the theory of diffusion-controlled chemical reactions. While earlier work was based on refinements of the enormously popular Smoluchowski concentration gradient theory or focused on the more formal aspects of the time evolution of an N-particle distribution function in some configuration space,[1-10] more recent developments have tended to emphasize the rather surprising and spectacular consequences of fluctuation-dominated kinetics; i.e., microscopic concentration fluctuations driven by random thermal fluctuations are magnified as the reaction progresses, so that an initially uniform system becomes macroscopically inhomogeneous and the concept of a reaction rate constant becomes invalid.[11-25]

By a combination of analytic theories and computer simulations, it has been discovered that a large variety of simple reactions exhibit this anomaly; and in fact, one is hard put to come up with an example of a diffusion-controlled reaction in which fluctuations do not, in some time regime, play a major role. The two most carefully studied examples are[13-25]

$$A + B \rightarrow \text{annihilation} \qquad (1.1a)$$

$$A + B \rightarrow B + C \qquad (1.1b)$$

the first being an irreversible bimolecular recombination (or annihilation) while the second is irreversible catalysis (B is the catalyst which transforms A into C). Not surprisingly, the spatial dimensionality d (Euclidian or fractal) in which the reaction occurs is a key parameter, and there has been considerable emphasis on identifying the "upper critical dimension" d_c—the dimension at and above which fluctuations are not dominant and a mean field description is valid. Thus for reaction 1.1a $d_c = 4$, if the initial concentrations of A and B are equal, while for (1.1b) $d_c = \infty$ if the catalyst is immobile. Moreover, the long time decay kinetics

(1) Noyes, R. M. *Prog. React. Kinet.* **1961**, *1*, 129.
(2) Collins, F. C.; Kimball, G. E. *J. Colloid Sci.* **1949**, *4*, 425.
(3) Waite, T. R. *Phys. Rev.* **1957**, *107*, 463.
(4) Waite, T. R. *Phys. Rev.* **1957**, *107*, 471.
(5) Waite, T. R. *J. Chem. Phys.* **1958**, *28*, 103.
(6) Monchick, L.; Magee, J. L.; Samuel, A. H. *J. Chem. Phys.* **1957**, *26*, 935.
(7) Wilemski, G.; Fixman, M. *J. Chem. Phys.* **1973**, *58*, 4009.
(8) Calef, D.; Deutch, J. M. *Annu. Rev. Phys. Chem.* **1983**, *34*, 493.
(9) Keizer, J. *J. Phys. Chem.* **1982**, *86*, 5052.
(10) Weiss, G. H.; Rubin, R. J. *Adv. Chem. Phys.* **1982**, *52*, 363.
(11) Montroll, E. W.; Shlesinger, M. F. In *The Mathematics of Disordered Media*; Hughes, B. D., Ninham, B. W., Eds.; Springer-Verlag: Berlin, 1983; p 109.
(12) Shlesinger, M. F. *J. Chem. Phys.* **1979**, *70*, 4813.
(13) Toussaint, D.; Wilczek, *J. Chem. Phys.* **1983**, *78*, 2642.
(14) Zumofen, G.; Blumen, A.; Klafter, J. *J. Chem. Phys.* **1985**, *82*, 3198. These authors report that the Smoluchowski target flux model is valid for the annihilation reaction $A + A \rightarrow *$.
(15) (a) Kang, K.; Redner, S. *Phys. Rev. Lett.* **1984**, *52*, 955. (b) Kang, K.; Redner, S. *Phys. Rev. A* **1985**, *32*, 435.
(16) Bramson, M.; Lebowitz, J. L. *Phys. Rev. Lett.* **1988**, *61*, 2397.
(17) Klafter, J.; Blumen, A.; Zumofen, G. *J. Phys. Chem.* **1983**, *87*, 191.
(18) Ovchinnikov, A. A.; Zeldovich, Ya. B. *Chem. Phys.* **1978**, *28*, 215.
(19) Kang, K.; Redner, S. *Phys. Rev. A* **1984**, *30*, 2833. These authors report ln t/t behavior for the single particle density for $A + A \rightarrow A$, which is similar but not identical with the A–A annihilation reaction.
(20) Kac, M.; Luttinger, J. M. *J. Math. Phys.* **1974**, *15*, 183.
(21) Donsker, M. D.; Varadhan, S. R. S. *Commun. Pure Appl. Math.* **1975**, *28*, 525.
(22) Donsker, M. D.; Varadhan, S. R. S. *Commun. Pure Appl. Math.* **1979**, *32*, 721.
(23) Bulagurov, B. Ya.; Vaks, V. G. *Sov. Phys.—JETP (Engl. Transl.)* **1982**, *38*, 6281. Balagurov, B. Ya.; Vaks, V. G. *Sov. Phys.—JETP (Engl. Transl.)* **1974**, *38*, 968.
(24) Grassberger, P.; Procaccia, I. *J. Chem. Phys.* **1983**, *77*, 6281.
(25) Kayser, R. F.; Hubbard, J. B. *Phys. Rev. Lett.* **1983**, *51*, 79.

0022-3654/90/2094-0652$02.50/0